J Nanotechnol Res 2020; 2 (1): 010-024 *DOI: 10.26502/jnr.2688-85210013*

Review Article

Microwave Assisted Synthesis of Graphene/SnO_2 Nanocomposite and its Structural, Dielectric and Electrical Properties

Moheeta Khan[1, 2*], Azra Parveen[1]

[1]Department of Applied Physics, Z.H. College of Engg. and Tech., Aligarh Muslim University, U.P, India

[2]Department of Education, Aligarh Muslim University, Aligarh, India

[*]Corresponding author: Moheeta Khan, Department of Education, Aligarh Muslim University, Aligarh, 202002, India, Tel: +91 9456243162; E-mail: moheetakhan@gmail.com

Received: 17 December 2019; **Accepted:** 28 December 2019; **Published:** 11 January 2020

Citation: Moheeta Khan, Azra Parveen. Microwave Assisted Synthesis of Graphene/SnO_2 Nanocomposite and its Structural, Dielectric and Electrical Properties. Journal of Nanotechnology Research 2 (2020): 010-024.

Abstract

Graphene-metal nanocomposites are the best candidates for the greater sensitivity for various applications. We have prepared Graphene-Tin Oxide (G/SnO_2) nanocomposite by using facile eco-friendly Anton-Paar microwave synthesis reactor method. X-ray diffraction patterns revealed the formation of G/SnO_2 nanocomposite. The scanning electron microscopy and transmission electron microscopy images show a uniform distribution of nano-needles on the graphene surface and the average particle size was found to be in the range of 3-5 nm. The G/SnO_2 composite shows an enhanced optical property, i.e., tunability in the band of pristine SnO_2 nanoparticles while in contacted with graphene. The dielectric properties of the G/SnO_2 nanocomposite were measured in the frequency ranges of 75Hz to 4MHz and real value of dielectric constant is found to be 1200, which is quite larger than that of pristine SnO_2 nanoparticle, i.e., 12. Further, AC conductivity analysis revealed that the G/SnO_2 is two orders conductive than the pristine SnO_2. This work may offer an effective and economically viable for the preparation of graphene/metal-oxide nanocomposites for various applications.

Keywords: Eco-friendly method; Graphene; Nanocomposite

1. Introduction

Over the decade, graphene has emerged as a promising nano-platform with enormous potential for biomedical

applications and translational research because of its excellent physical, chemical, and mechanical properties [1-4]. Graphene is a novel two-dimensional nano-material composed of sp^2-bonded carbon atoms, possesses a number of extraordinary electronic, optical, and thermal properties. A lot of interesting work has been carried out to explore the graphene for widespread biomedical applications, ranging from drug/gene delivery, biological sensing and imaging, antibacterial materials, to biocompatible scaffold for cell culture [3-5]. It is also known to have tremendous kind of properties such as high mobility of charge carriers of ~2×10^5 cm^2 $V^{-1}s^{-1}$ with intrinsic biocompatibility, low cost and scalable production, and facile biological/chemical functionalization [6].

As a new kind of carbon material, graphene has shown a wealth of exceptional properties and a variety of promising potential applications. Moreover, graphene is also established as composites with several semiconducting and metal oxides [7]. For example, Graphene-Tin Oxide (G/SnO_2) nanocomposite, which has been explored as an efficient material for Lithium-ion batteries application [8]. It is notably that there are few studies related to the Graphene with SnO_2 for different applications [8-11]. Hence, this require to develop reliable, facile and environmental-friendly methods to synthesize this nanocomposite. Generally, the synthesis methods of G/SnO_2 nanocomposite were either tedious (including synthesizing graphene sheets and preparing nanocomposites) or needed dangerous reagents. In this work, we have performed a detailed analysis on graphene/SnO_2 nanocomposite system by using SnO_2 as a model semiconductor and development of Eco-friendly Green Synthesis method. The in-situ growth of SnO_2 leads to the formation of uniform nanoparticles on graphene oxide (GO). Further, the SnO_2 formation helps to prevent not only the aggregation of the GO but also the aggregation of SnO_2 nanoparticles.

2. Synthesis of Graphene-SnO_2 Nanocomposite

2.1 Preparation of graphene Oxide

A concentrated H_2SO_4 (100 mL) was added to a mixture of graphite flakes (3.0 g, 1 wt. equivalent) and HNO_3 (25 mL), and the mixture was cooled to 0°C. $KMnO_4$ (9.0 g, 3 wt. equivalent) was added slowly in portions to keep the reaction temperature below 20°C. The reaction was warmed to 35°C and stirred for 30 min and simultaneously water (130 mL) was added slowly, producing a large exotherm to 90°C. External heating was introduced to maintain the reaction temperature at 90°C for 15 min and cooled down the reaction using a water bath for 10 min. Additionally, water (420mL) and 30% H_2O_2 (3mL) were added, producing another exotherm. After air cooling, the mixture was purified (sifting, filtration, multiple washings, centrifugations and decanting, vacuum drying) and left with the 1.2 g of solid graphene oxide i.e., GO.

2.2 Preparation of graphene/SnO_2 (G/SnO_2) composite

To synthesize G/SnO_2 nanocomposite, 0.2 g of GO and 0.7 g (2 mmol) of $SnCl_45H_2O$ were added to 60 mL of de-ionized water followed by sonication for 30 min. Then, 50 mL of hydrazine monohydrate (80 wt. %) was added to mineralize the tin (Sn) ions. After 15 min of stirring (at 70°C), the mixture was transferred into the Anton pear monoreactor with a capacity of 30 mL and reacted under hydrothermal conditions at 200°C for 1h. The Anton paar monowave reactor was slowly cooled down to room temperature, and a black-colored product (i.e., G/SnO_2) was isolated by filtration and dried at 60°C for 12 h. The whole synthesis process is demonstrated in schematically in Figure 1.

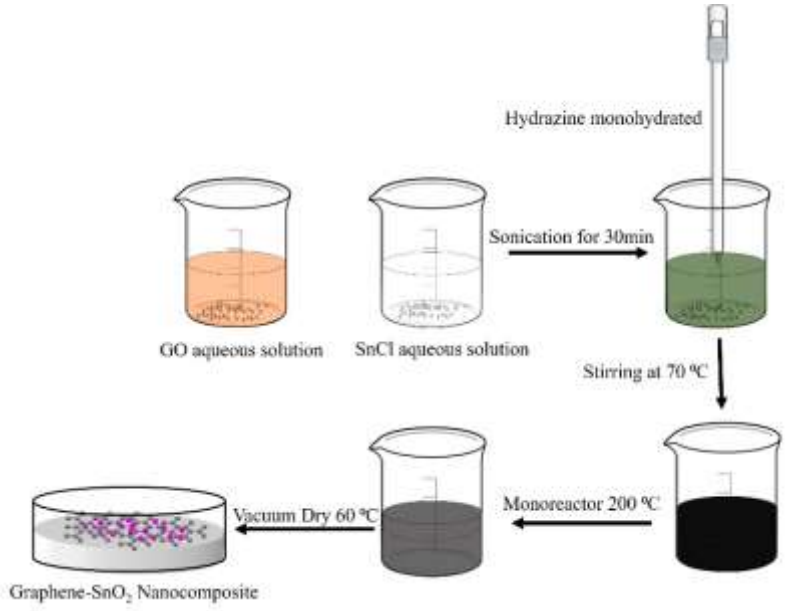

Figure 1: Formation mechanism of G/SnO_2 nanocomposite.

3. X-ray Diffraction (XRD)

Figure 2 show the XRD patterns of graphene oxide (GO), SnO_2 nanoparticle, and G/SnO_2 nanocomposite. The diffraction peaks of crystalline SnO_2 nanoparticles are clearly distinguishable. All strong diffraction lines can be indexed to the standard tetragonal SnO_2 phase (JCPDS card no. 41-1445), indicating their strong crystalline nature. For pure GO, (002) reflection at 2θ = 10.480^0 indicating a pure GO consists of multi-graphene oxide layer stacked together confirms from the other reports[8]. Further, GO is indeed reduced during hydrazine treatment. This diffraction peak around 10.480° for GO was shifted to a higher angle of around 24.475°, indicating that the GO was reassembled into graphene nanosheets (GNs). It can be noticeable in the G/SnO_2 nanocomposite which shows diffraction peaks of SnO_2 and G which shows agglomeration of GNs and SnO_2 nanoparticles. The mean crystallite size of bare SnO_2 and G/SnO_2 are estimated to be 34 nm and 21.42 nm based on the Debye Scherrer formula[12].

$$D = \frac{k\,\lambda}{\beta\,cos(\theta)}$$

Where, 'D' is the crystalline size of the particle, k is structure factor which is taken to be 0.94 for the crystalline systems, 'λ' is wavelength of Cu-K_α, 'β' is full width at half maxima and 'θ' is the diffraction angle. The shrink of the particle size of SnO_2 is understandably due to the confinement of graphene sheet.

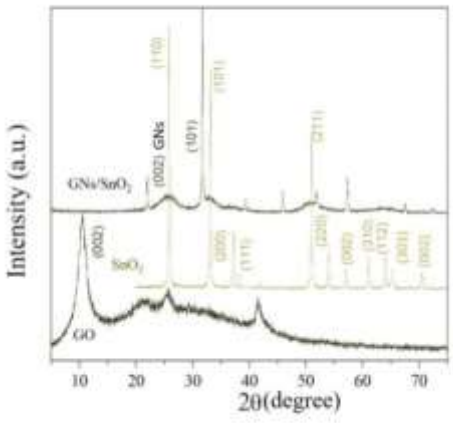

Figure 2: XRD patterns of SnO_2, GO and G/SnO_2 nanocomposite.

4. Scanning Electron Microscopy (SEM)

Figure 3 show the SEM images for G/SnO_2 nanocomposite sample. It reveals that the G/SnO_2 has a wavy shape consisting of various sheets arranged in a disordered manner while it seems that the tiny SnO_2 nanoparticles homogeneously distributed on the graphene nanosheets. It is visible that the shape of graphene is crumpled paper-like and has many folded edges which also show agglomeration of carbon nanoparticles as predicted by XRD discussed in the prevision section. These results show that the SnO_2 nanoparticles can be uniformly distributed on graphene through the interaction between graphene and SnO_2 nanoparticles [6, 13]. Figure 3(c) shows the corresponding energy-dispersive X-ray spectrum (EDS) of GNs/SnO_2 samples. Only Sn, C, and O elements are detected which further proves that there is no other impurities present in the sample. EDS elemental mappings for the elements Sn, O and C are shown in Figure 3 (d-f). The bright regions correspond to the presence of the elements Sn, O and C and indicate that the elements are distributed uniformly throughout the sample. The background signal in C mapping comes from the carbon conductive tape used to stick the sample with the sample holder.

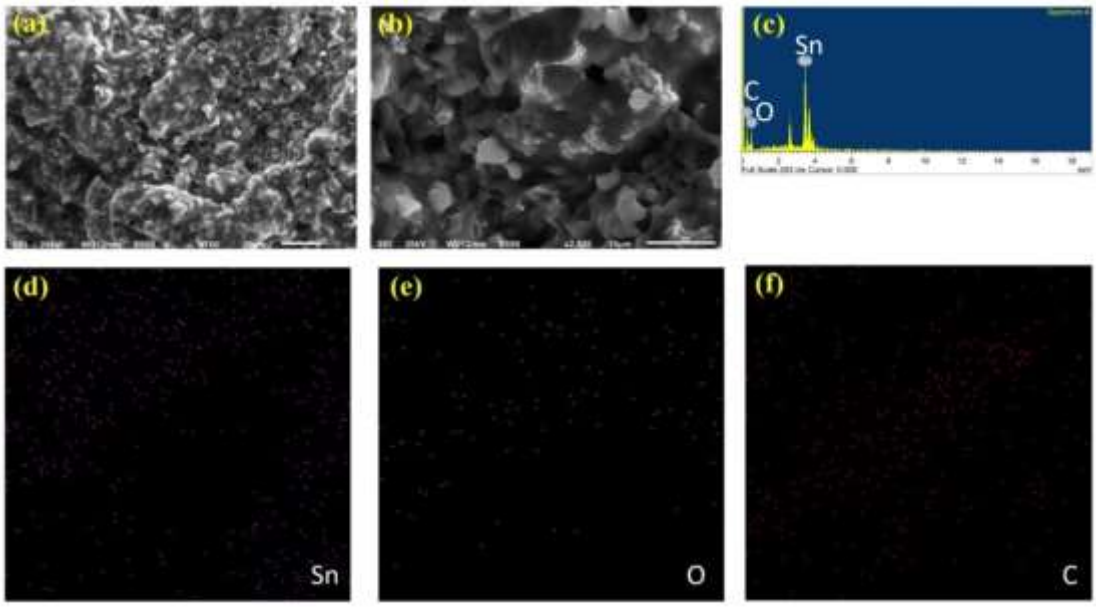

Figure 3: (a-b) Homogeneous distribution of SnO_2 nanoparticles on G; (c) Energy-dispersive X-ray spectrum; (e-f) are the elemental mapping of Sn, O and C.

5. Transmission Electron Microscopy (TEM)

Figure 4 shows the images acquired at the edges of G/SnO_2 composites. The composites are formed by several graphene sheets stacked together with SnO_2 particles needle like shaped homogeneously dispersed at their surface (dark shapes). In TEM images, it appears that the SnO_2 nanocrystals are distributed on the surface of the graphene nanosheets and the diameters of the SnO_2 nanorods are measured to be less than 16 nm which is in good agreement with XRD data analysis. In Figure. 4(b), two distinct signatures exhibits such as void contain graphene sheets and needle like shape of SnO_2. The former is due to the stacked and curled graphene sheets few layers as can be seen in Figure 4 (d), whereas in the latter, the SnO_2 nano-needle surrounded by graphene sheets. The voids between them come from monolayer sheet that are not completely anchored by SnO_2 nano-needle Figure 4 (c).

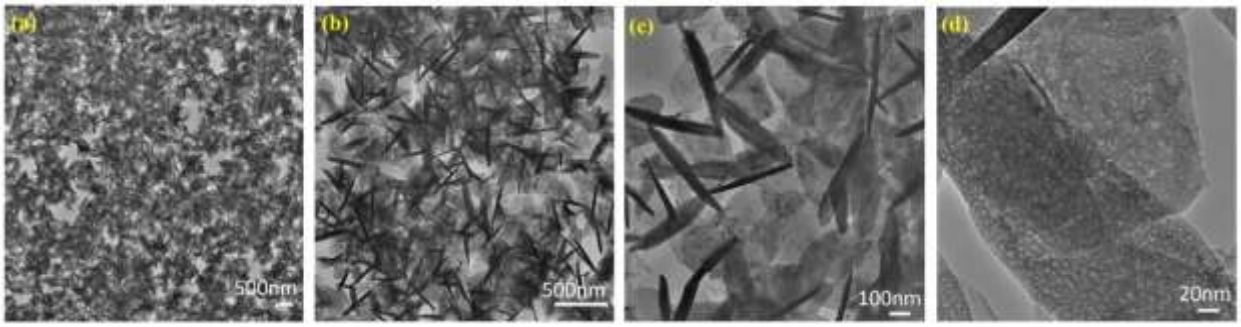

Figure 4: (a) Graphene interaction with SnO_2 Nano-needle. (b) Edges of GNs/SnO_2 nanocomposites. (c) Graphene sheet and SnO_2 Nano-needle. (d) Graphene sheets of few layers.

6. UV-Visible Spectroscopy

Energy emission of grown nanoparticles were analyzed by UV-Vis spectroscopy. Figure 5 shows the UV-Vis spectra of G/SnO_2 nanocomposite, GO and SnO_2 nanoparticles samples. As excepted, GO exhibits strong band centered at 230 nm, corresponding to π–π* transitions of the aromatic C═C band. It is clearly seen that the absorption peak shifted to 250 nm indicating the reduction of GO and that the product is capable of absorbing visible light. These results shows the endorsement synthesis of G/SnO_2 nanocomposite. The electronic band gap (E_g) of the SnO_2 and G/SnO_2 nanocomposite were determined by employing *Tauc* relationship,

$$\alpha h\nu = B\left(h\nu - E_g\right)^{1/2}.$$

Where $h\nu$ is the photon energy, α is the absorption coefficient, and B is constant. The absorption coefficient can be written as $\alpha = 2.303A/t$, where A is absorbance and t is the thickness of the cuvette used in the measurement. Figure 5 (a) shows the UV-Vis absorption spectra from three different samples where the absorption peaks corresponds to the GO and G/SnO_2 clearly differentiate the band gap energies. The $(\alpha h\nu)^2$ vs energy gap E_g shown in Figure 5(b) and the extrapolation of the linear region on the X-axis gives the values of the optical band gap. The values of E_g of the SnO_2 is found to be 3.85 eV which is matched with the reported results [14, 15]. The red shift was observed for G/SnO_2 nanocomposite and band gap energy was estimated to be 3.66 eV. Reduction of band gap of bare SnO_2 nanoparticles by introducing of graphene sheet (a zero band gap system) effectively introduced metastable stages among the valence and conduction bands.

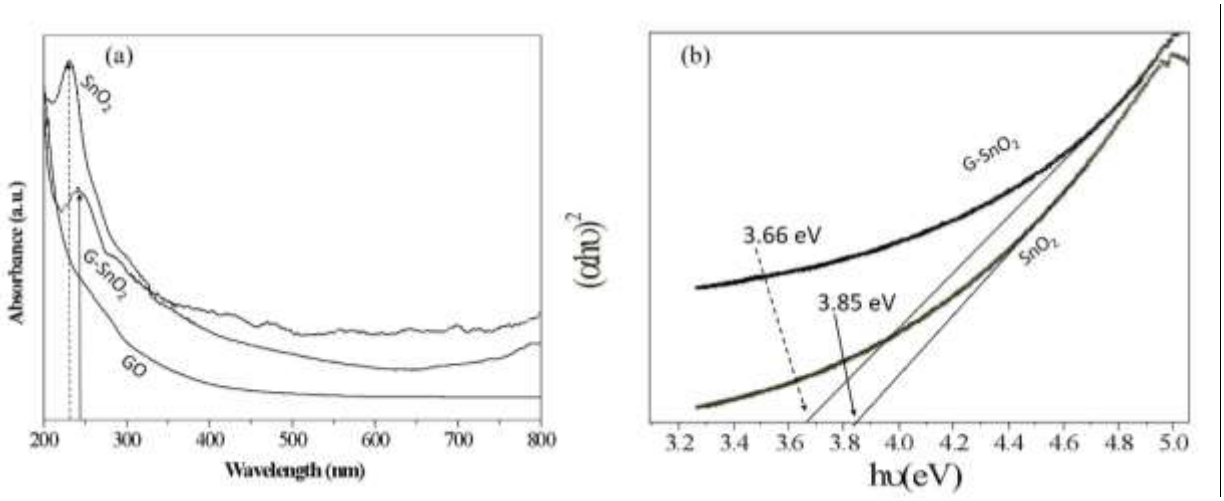

Figure 5: (a) UV-Vis spectrograph of SnO_2, GO and G/SnO_2 nanocomposite. (b) $(\alpha h\nu)^2$ vs. E_g plot for bandgap energy calculation.

7. Fourier Transform Infrared (FTIR): Functional Analysis

Figure 6 shows the fingerprint of bonding in the GO, SnO and G/SnO_2 nanocomposite systems. We are mainly interested to look the vibrational bonds of formation of graphene from GO when it reduced while it contacted with SnO_2 nanoparticles. Peak around 3450 cm^{-1} is attributed to O-H stretching vibrations of adsorbed water molecules and structural OH groups which exhibits with large intensity in SnO_2 nanoparticles and broader in GO due to large oxygen environment but it get reduced to G/SnO_2

nanocomposite. The C-O stretching vibration observed around 1080 cm^{-1} which is not present in the nanocomposite sample which means the formation of G in nanocomposite sample [16] and confirm the adhesion of the graphene to SnO_2 nanoparticles as discussed in the previous sections. Moreover, on adding SnO_2 into the GO solution, a strong Sn-O-Sn anti-symmetric vibration peak is observed at 585 cm^{-1} which resemble to bare SnO_2 nanoparticle corresponding change in nanocomposite [15]. No bonding confirmation is observed between graphene and SnO_2. Further, it is important to see that the peaks of carboxyl group suppressed significantly and a new peak at 1640 cm^{-1} appears, corresponding to the skeletal vibration of graphene [17].

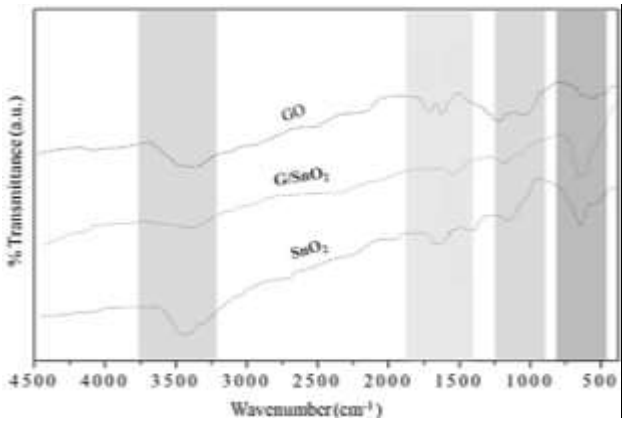

Figure 6: FTIR spectra recorded of GO, SnO_2 nanoparticles and G/SnO_2 nanocomposite samples.

8. Thermal Analysis: DSC and TGA

The DSC analysis consists in measuring the difference in heat flow between the sample and a reference (inert material) when both are submitted to the same temperature ramp. The DSC plots for both of the samples G/SnO_2 and SnO_2 in the Figure 7 (right panel) shows their exothermic nature, which results when the samples were heated at a rate of 5ºC/min. From 40ºC to 400ºC in nitrogen gas flowing at a rate of 25ml/min. For SnO_2 nanoparticle, the DSC plot gives only one exothermic peak at 290ºC, which indicates change of phase at the temperature. While for G/SnO_2 nanocomposite two exothermic peaks exists, one peak correlated to Graphene nanosheets at 70ºC and the peak at 270ºC corresponding to SnO_2 nanoparticles. The corresponding change in temperature of nanocomposite on comparing to bare SnO_2 nanoparticle also verifies the conformation of the synthesis of G/SnO_2 nanocomposite [18]. The thermal properties and the compositions of the as-prepared products were characterized by TGA in air environment. TGA curves of the G/SnO_2 nanocomposites and SnO_2 nanoparticle are shown in Figure 7 (left panel). An abrupt weight loss occurs from 200ºC to 650ºC, indicating the oxidization of G/SnO_2 nanocomposite, and no further mass loss is observed after 650ºC. In the spectrum weight loss show in two patterns, first pattern from 200ºC to 300ºC showing the SnO_2 weight loss, mainly caused by its dehydration, which can also be verified through alone SnO_2 i.e. SnO_2 shows the weight loss in the temperature region 200ºC to 300ºC with 60 weight % and second pattern 350ºC to 650ºC shows the weight loss with 30 weight % of carbon as a result of pyrolysis. The stability of the trace indicates the complete removal of graphene. According to the TGA curves, 53 wt% of SnO_2 are coated on the surface of graphene nanosheets.

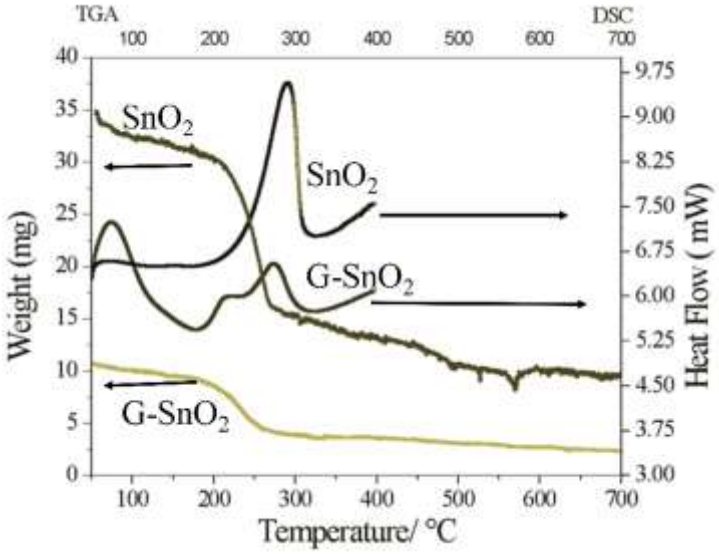

Figure 7: TGA(left panel) and DSC(right panel) of SnO_2 and G/SnO_2.

9. Frequency Dependent Electrical Properties

9.1 Dielectric constant

The dielectric constant is represented as ε = ε′- *j*ε″. The first term is the real part of dielectric constant and describes the stored energy while the second term is the imaginary part of dielectric constant, which describes the dissipated energy. The dielectric constants ε′ and ε″ of the materials were evaluated by using the relation,

$$\epsilon' = \frac{C_p t}{A\epsilon_0}$$

and $\epsilon'' = \epsilon' \times tan\delta$.

Where ϵ_0 is the permittivity of free space, C_p is the capacitance of the specimen, *A* and *t* are the flat surface area and thickness of the pallet, respectively. Here $tan\delta$ represents the dialectic loss. Figure 8 show the real (ε′) and imaginary (ε″) part of dielectric constant of both the samples. The ε′ and ε″ values of SnO_2 (G/SnO_2) were found to be 15-9 (1200-1000) and 12-7(14000-1000), respectively. From figures, it is noticeable that a sudden

decrease in lower frequency regime and become slower at higher frequency. The trend of decrease in the dielectric constant with increasing frequency is due to by dielectric relaxation phenomenon, which tells that the charge carrier localization is not stable and frequency disturbances affect the charge carrier. In other words, a phenomenon of electron-hopping mechanism is also responsible where it is prominent at higher frequency that results in reduction of the dielectric constant [19]. Further, it is seen that the value of ε′ decreases faster compared to that of ε″. A larger value of ε″ in case of G/SnO_2 nanocomposite shows the large heat dissipation. Thus, the present nanocomposite exhibits conducting behavior due to presence of graphene nanosheets. Further, the dielectric dispersion curve can also be explained based on Koop's theory [20], which is based on the Maxwell-Weigner model [21, 22] for the homogeneous double structure. According to this model, a dielectric medium is assumed to be made of well conducting grains that are separated by poorly conducting (or resistive) grain boundaries. Under the application of external electric field, the charge carriers can easily migrate through the grains and accumulated at the grain boundaries. This process can produce large polarization and high dielectric constant. The small conductivity of grain

boundary contributes to the high value of dielectric constant at low frequency. The higher value of dielectric constant can also be explained on the basis of interfacial/space charge polarization due to inhomogeneous dielectric structure, i.e. may be porosity and grain structure of nanocomposite. The polarization decreases with the increase in frequency and then reaches a constant value beyond a certain frequency. It is understandably that in an external field the hopping phenomena occurs between graphene & SnO_2 and shows the recombination effect of electron and holes which cannot follow the alternating field. The large value of dielectric constant at lower frequency is due to the predominance of the effect like grain boundary defects, presence of oxygen vacancies, etc. Further, the decrease in dielectric constant with frequency is natural because of the fact that any species contributing to polarizability is found to show lagging behind the applied field at higher and higher frequencies.

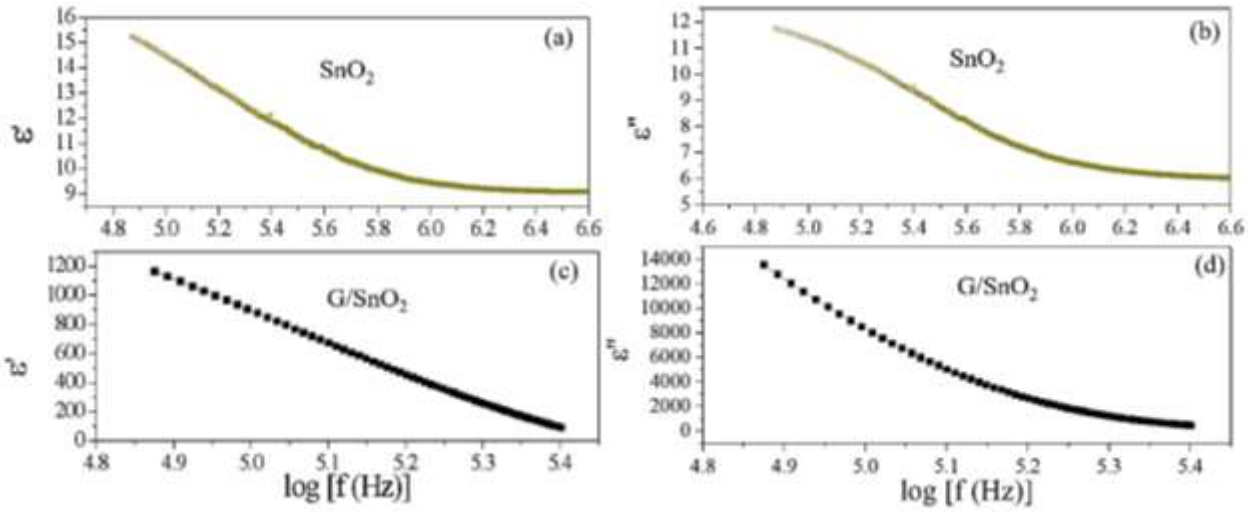

Figure 8: (a), (c), (b) and (d) are the variation of real and imaginary part of the impedance with frequency for SnO_2 nanoparticles and G/SnO_2 nanocomposite.

9.2 Dielectric losses

Figure 9 shows the SnO_2 and G/SnO_2 nanocomposite exhibited the frequency dependent dielectric losses. At higher frequency, the losses are constant but large in G/SnO_2 nanocomposite as compared to the SnO_2 nanoparticles because of the smaller particle size as confirmed form the structural analysis as discussed in the previous section. The high value of dielectric losses at lower frequency may due to the high resistivity caused by grains boundary. The low loss in G/SnO_2 nanocomposite as compared to the SnO_2 shows the capability of G/SnO_2 to use in high frequency device applications.

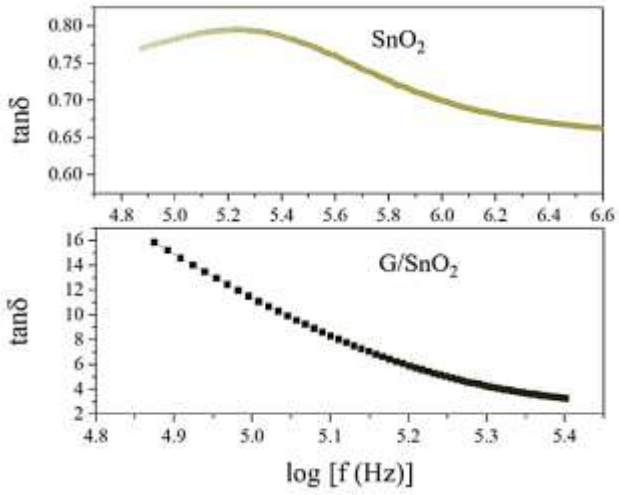

Figure 9: Variation of dielectric losses with frequency.

9.3 AC conductivity

The total conductivity can be explained as,

$\sigma_{tot} = \sigma(T) + \sigma(\omega, T)$.

The first term represents the dc conductivity due to the band conduction that is frequency independent and the second term is the pure ac conductivity due to the electron hopping processes. Figure 10 shows the variation in ac conductivity with frequency for SnO_2 and G/SnO_2 nanocomposite measured at room temperature. The ac conductivity is quite large (more than one order) in G/SnO_2 nanocomposite as compared to the SnO_2 nanoparticles. It is due to small particle size of G/SnO_2 nanocomposite that comprise graphene ballistic conductivity, less defect and small grain boundary. Due to this, as the frequency increases electron-hoping process increases and shows a sharp increment in the ac conductivity compare the SnO_2 nanoparticle attributed to the enhanced electron hopping phenomenon [23].

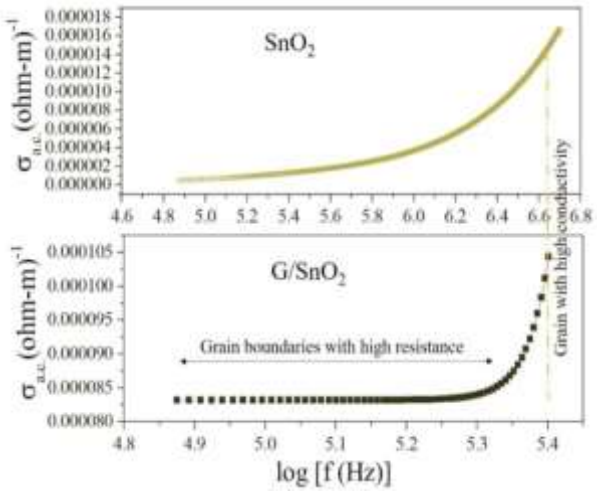

Figure 10: Variation of ac conductivity with frequency.

9.4 Impedance analysis

It is an imperative tool to separate the bulk and grain boundary contribution by from the total conductivity. The impedance spectrum is represented as imaginary (Z") versus real component of impedance (Z') and known as Nyquist plot [23]. In that, at higher and lower frequencies represent bulk and electrode process, respectively, while that at intermediate frequencies represents grain boundary contribution. For the detailed investigation of the transport properties of as prepared SnO_2 nanoparticles and G/SnO_2 nanocomposite, the impedance measurement was performed in the frequency range of 75Hz-4 MHz at room temperatures. The complex formalism of the impedance is given by the relation,

$$Z^* = Z' - i\,Z'' = R_S - \frac{1}{j\omega C_S}$$

The electrical phenomenon due to bulk material, grain boundary and interfacial phenomenon appears in the form of arc of a semicircle, when components of impedance are plotted in a complex argand planes (Nyquist plots) [23]. Figure 11 shows the variation of real and imaginary part of the impedance with frequency for SnO_2 nanoparticles and G/SnO_2 nanocomposite. It has been clearly visible from the patterns that Z' decreases with the increase in frequency for both the samples (Figure 11(a) and (c)). This reduction with the rise in frequency is due to the increase in ac conductivity with rise in frequency as discussed in the previous section. It may also attributed to high resistivity due to effectiveness of the resistive grain boundaries in the low frequency region and shows independent behavior in the higher frequency region. It may be noticed that the Z' decreases with decreasing particle size.

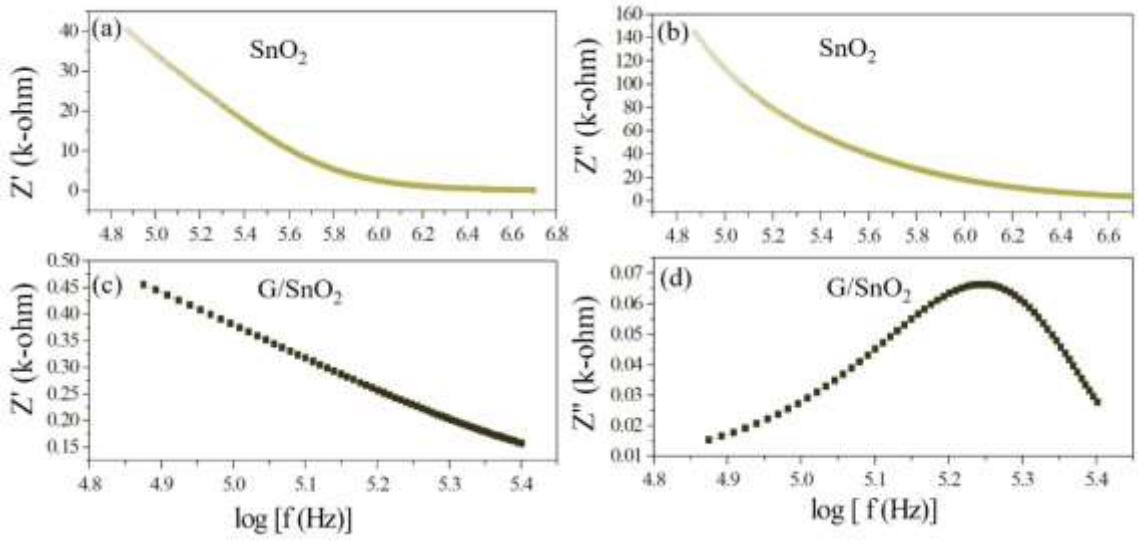

Figure 11: (a) (c) and (b) and (d) are the variation of real and imaginary part of the impedance with frequency for SnO_2 nanoparticles and G/SnO_2 nanocomposite.

Furthermore, the Z" decreases with the decreasing particle size due to capacitance of grain boundary (Cgb) as shown in the Table 1 below,

Sample	R_{gb} (Ω)	C_{gb} (nF)	τ_{gb}(×10^{-6} s)
G/SnO_2 Nanocomposite	0.46284	181.58	84.0424872
SnO_2	1860.9	1.1063	2058.71367

Table 1: Parameters are obtained by analyzing the impedance data on nonlinear least square fit method.

This can be attributed to the fact that Z'' is inversely proportional to capacitance by the relation, $Z'' = 1/j\omega C_S$. Moreover, Z' and Z'' are given by the relations,

$$Z' = \frac{R_g}{1+\left(\omega_g^2 C_g^2 R_g^2\right)} + \frac{R_{gb}}{1+\left(\omega_{gb}^2 C_{gb}^2 R_{gb}^2\right)}$$

$$Z'' = \frac{R_g \omega_g C_g}{1+\left(\omega_g^2 C_g^2 R_g^2\right)} + \frac{R_{gb}\omega_{gb} C_{gb}}{1+\left(\omega_{gb}^2 C_{gb}^2 R_{gb}^2\right)}$$

.Where R_g, R_{gb}, C_g, C_{gb} are the resistance and capacitance of grain and grain boundary respectively, while ω_g and ω_{gb} are the frequencies at the peaks of the circular arc for the grain and grain boundary respectively. The capacitance and the relaxation times (τ_g, τ_{gb}) were calculated for the grain and grain boundary by using the relations, $C_g = 1/R_g\omega_g, C_{gb} = 1/R_{gb}\omega_{gb}, \tau_g = R_g C_g, \tau_{gb} = R_{gb}C_{gb}$. Grain boundary resistance R_{gb} increases while the capacitance C_{gb} decreases with decreasing particle size as indicated in the table 1. This is due to smaller grains imply a larger number of insulating grain boundaries which act as a barrier to the flow of electrons. Smaller grains also imply smaller grain–grain surface contact area and therefore a reduced electron flow. Figure 12 shows the complex impedance plots (Nyquist plot) for the samples SnO_2 and G/SnO_2 nanocomposite. Generally, the grains are effective in high frequency region while the grain boundaries are effective in low frequency region. The size of the semicircle changes with grain size and the number of grains. The presence of a single semicircular arc obtained at higher frequencies corresponds to electrical conduction by the interior of the bulk grain. The diameter of the semicircle corresponds to the resistance of the grain. Accordingly, the semicircle at high and low frequencies may be assigned to charge transport within the crystallites and a grain boundary effect, respectively [24].

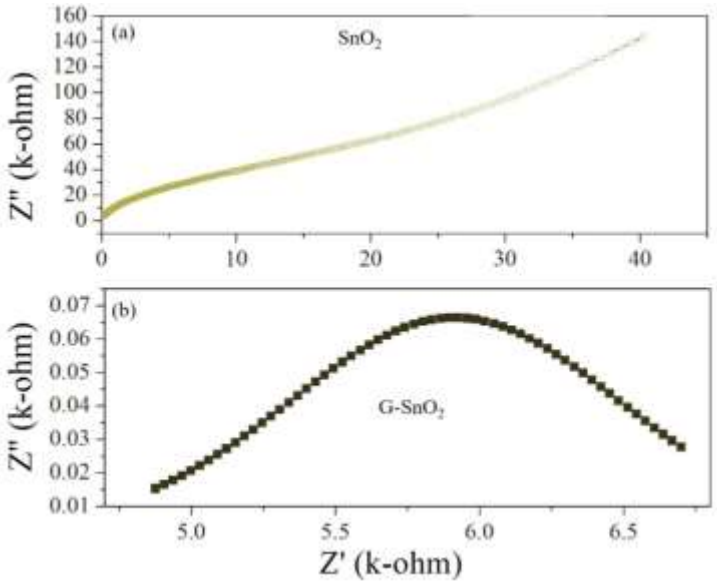

Figure 12: Nyquist plot of SnO_2 and G/SnO_2.

In general, the grain boundary effect on electrical conductivity may originate from a grain boundary potential barrier or from space charge layers which are depleted in majority charge carriers and which are localized along the grain boundaries [23-25]. However, a low frequency semicircle may also be an artifact caused by porosity, which is known as the constriction. As the particle size decreases, the diameter of the semicircle increases, indicating a reduction of the grain interior resistance. Due to this fact, the single circular arc is being observed in these Cole-Cole plots. Moreover, it can be seen from Figure 12 (Nyquist plot) that total impedance increases with decreasing particle size of the sample which is in well agreement with conductivity analysis.

10. Conclusions

A simple facile eco-friendly Anton-Paar microwave synthesis reactor approach has been utilized for the controlled growth of SnO_2 nanoparticles onto graphene layer. X-ray diffractions and scanning electron microscopy analyses revealed the growth of graphene/SnO_2 nanocomposite. XRD patterns revealed diffraction peaks corresponding to SnO_2, graphene oxide, graphene G/SnO_2 nanocomposites. The nanocomposites were successfully synthesized without any impurities. According to the SEM and TEM observation, the uniform distribution of the nano-needles on the graphene surface is demonstrated with average particle size of 3-5 nm extracted. According to the TGA, 53 wt. percentage of SnO_2 are coated on the surface of graphene nanosheets. Based on the electrical measurements, the G/SnO_2 nanocomposite behave highly conducting as compared to the SnO_2 nanoparticles. The G/SnO_2 nanocomposite composite showed an enhanced optical property, tuning of band of bare SnO_2 nanoparticles. These features with the green synthesis make the G/SnO_2 nanocomposites an excellent material for various applications such as research fields such as biosensor, gas sensor, ultracapacitors, and electrochemical analysis.

Acknowledgements

We acknowledge the Centre of Excellence in Materials Science (Nanomaterials), Department of Applied Physics, Z.H. College of Engineering & Technology, Aligarh Muslim University, Aligarh, Uttar Pradesh, India for the financial support for completing the presented work.

Conflicts of Interest

All authors declare no competing interests.

References

1. Rao CNR, Sood AK, Subrahmanyam KS, Govindaraj A. Graphene: The new two-dimensional nanomaterial, Angew. Chemie - Int. Ed 48 (2009): 7752-7777.
2. Teweldebrhan D, Lau CN, Ghosh S, Balandin AA, Bao W, Calizo I, et al. Superior Thermal Conductivity of Single-Layer Graphene. Nano Lett 8 (2008): 902-907.
3. Ge Z, Jin Z, Fan H, Zhao K, Wang L, Shi Z, et al. Fabrication, Mechanical Properties, and Biocompatibility of Graphene-Reinforced Chitosan Composites. Biomacromolecules 11 (2010): 2345-2351.
4. Cheng C, Li S, Thomas A, Kotov NA, Haag R. Functional Graphene Nanomaterials Based Architectures: Biointeractions, Fabrications, and Emerging Biological Applications. Chem. Rev 117 (2017): 1826-1914.
5. Shen H, Zhang L, Liu M, Zhang Z. Biomedical applications of graphene. Theranostics 2 (2012): 283-294.
6. Guo S, Dong S. Graphene nanosheet: Synthesis, molecular engineering, thin film,

hybrids, and energy and analytical applications. Chem. Soc. Rev 40 (2011): 2644-2672.

7. Yang X, Tu Y, Li L, Shang S, Tao XM. Well-dispersed chitosan/graphene oxide nanocomposites. ACS Appl. Mater. Interfaces 2 (2010): 1707-1713.
8. Liang J, Wei W, Zhong D, Yang Q, Li L, Guo L. One-step in situ synthesis of Snow 2 /graphene nanocomposites and its application as an anode material for Li-ion batteries. ACS Appl. Mater. Interfaces. 4 (2012): 454-459.
9. Pi S, Zhang X, Cui H, Chen D, Zhang G, Xiao S, et al. Facile Fabrication of Au Nanoparticles/Tin Oxide/Reduced Graphene Oxide Ternary Nanocomposite and Its High-Performance SF_6 Decomposition Components Sensing, Front. Chem 7 (2019): 1-13.
10. Zhang B, Yu X, Ge C, Dong X, Fang Y, Li Z, et al. Novel 3-D superstructures made up of SnO_2@C core-shell nanochains for energy storage applications, Chem. Commun 46 (2010): 9188-9190.
11. Li F, Song J, Yang H, Gan S, Zhang Q, Han D, et al. One-step synthesis of graphene/SnO_2 nanocomposites and its application in electrochemical supercapacitors, Nanotechnology 20 (2009): 455602.
12. Husain S, Rahman F, Ali N, Alvi PA. Nickel Sub-lattice Effects on the Optical Properties of ZnO Nanocrystals, J. Optoelectron. Eng 1 (2013) 28-32.
13. Song J, Xu L, Zhou C, Xing R, Dai Q, Liu D, et al., Synthesis of graphene oxide based cuo nanoparticles composite electrode for highly enhanced nonenzymatic glucose detection, ACS Appl. Mater. Interfaces 5 (2013): 12928-12934.
14. FJ Arlinghaus. Energy bands in stannic oxide (SnO_2). J. Phys. Chem. Solids 35 (1974): 931-935.
15. Chetri P, Choudhury A. Investigation of optical properties of SnO_2 nanoparticles. Phys. E Low-Dimensional Syst. Nanostructures 47 (2013): 257-263.
16. Çiplak Z, Yildiz N, Cąlimli A. Investigation of graphene/Ag nanocomposites synthesis parameters for two different synthesis methods, Fullerenes Nanotub. Carbon Nanostructures 23 (2015): 361-370.
17. Si W, Wu X, Zhou J, Guo F, Zhuo S, Cui H, et al. Reduced graphene oxide aerogel with high-rate supercapacitive performance in aqueous electrolytes, Nanoscale Res. Lett 8 (2013): 247.
18. Shanmugam M, Jayavel R. Synthesize of Graphene-Tin Oxide Nanocomposite and Its Photocatalytic Properties for the Degradation of Organic Pollutants Under Visible Light. J. Nanosci. Nanotechnol 15 (2015): 7195-7201.
19. Zhu J, Wei S, Zhang L, Mao Y, Ryu J, Haldolaarachchige N, et al. Electrical and dielectric properties of polyaniline-Al_2O_3 nanocomposites derived from various Al_2O_3 nanostructures. J. Mater. Chem 21 (2011): 3952-3959.
20. Koops CG. On the dispersion of resistivity and dielectric constant of some semiconductors at audiofrequencies, Phys. Rev 83 (1951) 121–124.
21. Wagner KW. The theory of imperfect dielectrics. Ann. Phys 345 (1913): 817-855.
22. Yager WA. The distribution of relaxation times in typical dielectrics. J. Appl. Phys 7 (1936): 434-450.
23. Radoń A, Łukowiec D, Kremzer M, Mikuła J, Włodarczyk P. Electrical conduction mechanism and dielectric properties of

spherical shaped Fe_3O4 nanoparticles synthesized by co-precipitation method, Materials (Basel) 11 (2018): 735.

24. Mombrú D, Romero M, Faccio R, Tumelero MA, Mombrú AW. Extremely Large Magnetic-Field-Effects on the Impedance Response of TiO_2 Quantum Dots. Sci. Rep 9 (2019): 5322.
25. Hemalatha KS, Sriprakash G, Ambika Prasad MVN, Damle R, Rukmani K. Temperature dependent dielectric and conductivity studies of polyvinyl alcohol-ZnO nanocomposite films by impedance spectroscopy. J. Appl. Phys 118 (2015): 154103.